Kinetic Study of Low Temperature Sulfur Dioxide Removal Reaction By Sodium Carbonate Using Random Pore Model

Iman Omidi
Amirkabir University of Technology Department of Chemical Engineering
Habib Ale Ebrahim (alebrm@aut.ac.ir)
Amirkabir University of Technology Department of Chemical Engineering https://orcid.org/0000-0003-0947-9444

Research Article

Keywords: Sodium carbonate, SO2 removal, Kinetic study, Thermogravimetry, Random pore model

Posted Date: March 31st, 2021

DOI: https://doi.org/10.21203/rs.3.rs-324950/v1

Kinetic Study of Low Temperature Sulfur Dioxide Removal Reaction by Sodium Carbonate using Random Pore Model

Iman Omidi and Habib Ale Ebrahim*

Department of Chemical Engineering, Amirkabir University of Technology (Tehran Polytechnic), Tehran, Iran

Abstract

An experimental investigation of low temperature SO_2 removal by porous sodium carbonate was carried out by thermogravimetry. As well as, applied mathematical modeling based on the random pore model was employed to kinetic study of this reaction. The experiments were performed at various temperatures (100-250 ^oC) and different SO_2 concentrations (0.13-1.12 vol%). The initial slopes procedure was used to determine dependency of the reaction rate constants versus temperature. First-order kinetic with respect to gaseous reactant was found and value of activation energy was attained as 22.5 kJ mol^{-1}. Product layer diffusion coefficients were evaluated by the best fitting of experimental data with the model predictions. These random pore model predictions indicated good agreement with experimental conversion-time data at various conditions. The resulted kinetic parameters were avail abled for engineering calculations of SO_2 abatement from the coal-based power plants by low-temperature flue gas desulfurization.

Keywords:

Sodium carbonate; SO_2 removal; Kinetic study; Thermogravimetry; Random pore model

---

*: Corresponding author phone/fax: 00982166405847, Amirkabir University of Technology (Tehran Polytechnic), Departement of Chemical Engineering/Non-catalytic gas-solid reactions laboratory, Tehran, Iran, email: alebrm@aut.ac.ir

1. Introduction

1.1 Background Information

One of the significant air contaminant which causes acid rain is sulfur dioxide. Sulfuric acid formed by the reaction of SO_2 with water vapor in the air generates acid rain afterward. Creation of acidic lakes, reduction of soil fertility, damaging forests, and corrosive results on stones and metals are some of the acid rain's destructive impacts. Therefore, lots of industries require to develop appropriate SO_2 removal procedures because of the environmental hazards of this air pollutant.

Power plants based on coal, roasting units of extractive metallurgical plants (copper and zinc) and refineries of natural gas are the sulfur dioxide's major sources (Petheram 2002). Several SO_2 emission controller rules are established for the mobile sources. European Union limited the sulfur values in gasoline and gas-oil to 10 ppm since 2010 (Stanislaus et al. 2010). Consequently, modified catalysts have been presented for petroleum fuels hydrotreating (Chen et al. 2010, Yin et al. 2011). As well as to increase SO_2 removal yield from the stationary sources, recent studies focused on different Flue Gas Desulfurization (FGD) methods.

FGD technologies include throw-away and regenerative processes (Kirk et al. 1949). Throw-away procedures are suitable for based coal power plants within 1000 ppm SO_2 concentrations. The general sorbent in these processes is lime (CaO). However, lime reaction with sulfur dioxide is accomplished at high temperatures (about 800 ^oC). Moreover, incomplete conversion can be occurred owing to pore mouth obstruction (Z=3) (Ale Ebrahim 2010).

In addition, wet and dry regenerative processes are appropriate with high SO_2 concentrations in several metallurgical systems. SO_2 absorbs by Na_2SO_3 solution and strips in wet regenerative FGD method. In dry regenerative FGD method, $CuSO_4$ produced by the reaction of SO_2 with CuO. Then, CuO regenerated with reducing $CuSO_4$ by H_2. The concentrated SO_2 stream in both regenerative processes should be reduced by methane (Mousavi et al. 2018, Sohn &Kim 2002).

Metal oxides and metal carbonates are the current adsorbents of throw-away processes consist of CaO (lime), MgO, Na_2CO_3, K_2CO_3, Fe_2O_3, etc. The main characteristic of these processes are simplicity of operation and economic efficiency (Gray &Jarvis 2020, Jia et al. 2007, Tseng &Wey

2004). Major advantage of sodium carbonate is its ability to remove SO_2 at low temperatures (about 200 ^oC). The Na_2CO_3 sorbent base FGD reaction can be written as:

$$Na_2CO_3 + SO_2 + 0.5O_2 \rightarrow Na_2SO_4 + CO_2 \quad (1)$$

1.2 Literature Review

To investigate performance of sulfur dioxide removal by sodium carbonate several experimental studies have been done in the literature.

Dry sodium injection has been studied by the Electric Power Research Institute (EPRI) since 1977. This material tested as a solid sorbent (Bland 1990). The related test results demonstrate that SO_2 reduce 70-90% for subbituminous coals combustion with a different sorbents based on sodium, which all of them contain a considerable ratio of sodium bicarbonate.

Several studies were conducted to investigate the influence of $NaHCO_3$ thermal decomposition to Na_2CO_3 on SO_2 absorption efficiency (Carson 1980, Dal Pozzo et al. 2019, Erdos et al. 1989, Knight 1977, Mocek &Beruto 1986). These reports indicated that gas temperatures between 120-175 ^oC showed the best performance for SO_2 scrubbing when the initial substance is sodium bicarbonate.

Han et al. described for the first time that Na_2CO_3 additive can promote the sulfate conversion of limestone due to the enhanced surface area and tuned pore size distribution (Han et al. 2017). A packed scrubber with absorbents (limestone and sodium bicarbonate) was used by Ghorbani et al. to measure the concentration of sulfur dioxide at the inlet and outlet of scrubber. The results presented the more SO_2 removal efficiency by using these absorbents with cation surfactants (ghorbani shahna et al. 2017).

A non-isothermal thermogravimetric analysis was used by Wu et al. to determine the intrinsic kinetics of the $NaHCO_3$ to Na_2CO_3 decomposition reaction. They reported activation energy as 25.3 kcal mol^{-1} for sodium bicarbonate decomposition. They found that elevating the temperature of decomposition from 120 to 230 °C enhances pore diameter from 180 to 210 nm (Wu &Shih 1993).

Mortson et al. applied regenerated sodium bicarbonate/carbonate to remove SO_2 and NO_x using an advance and economic FGD technology developed by AIRborne Technologies Inc. (ATI). High SO_2 removal yield and production of different fertilizers reported in this work (Mortson &Telesz 2001).

Guangwen et al. used a powder-particle fluidized bed reactor to absorb SO_2 and NO by Na_2CO_3/Al_2O_3. As well as they examined different effective parameters, such as reaction temperature, fraction of mixtures in flue gas, and sorbent size (Xu et al. 2000).

Walawska et al. studied on structural factors of particle. In addition, mechanically and thermally activated sodium bicarbonate were considered. Sodium carbonate showed better removal yield than sodium bicarbonate (Walawska et al. 2014).

Ma et al. presented a concept test of NOXSO flue gas treatment process at three scales of 0.017, 0.06 and 0.75 MW power plants (Ma &Haslbeck 1993).

To explain the $NaHCO_3$ and SO_2 reaction, Keener et al. employed shrinking core model (with neglecting solid reactant porosity). In order to deduce the rate constant expression, kinetic data were exported from this model. The measured activation energy (56.4 $kJmol^{-1}$) indicates dependency of rate constant to temperature (Keener &Khang 1993).

Kimura et al. studied the SO_2-Na_2CO_3 reaction kinetics in the range of 80-140 ^oC, constant SO_2 concentration of 0.3% with thermogravimetric analysis data. Because of rapid reaction, particular precautions were affected to operate such that transport resistance did not change the results. Rate constants were estimated from the suggested mechanism and the experimental data (Kimura &Smith 1987). However, SO_2 diffusion resistance between Na_2CO_3 nano-grains was neglected (Kimura &Smith 1987).

Ebrahimi et al. developed a model based on film theory for the SO_2 removal by $NaHCO_3/Na_2CO_3$ solution in a packed tower. This model includes diffusion and reaction processes, also thermodynamic equilibrium was considered for reactants in the bulk fluid (Ebrahimi et al. 2003).

Prada et al. designed a fixed-bed reactor to remove SO_2 in flue gases with sodium bicarbonate. Experiments were performed for 1500 ppm SO_2 and temperatures above 122 ^oC. In addition, a solution technique was used to predict the performance of reaction in this system with respect to

the length of reactor. This work showed better economic efficiency than SO_2 elimination with activated carbon for small-scale FGD applications (Charry Prada et al. 2019).

1.3 Goals and Importance of the Present Study

As mentioned, lime-based FGD systems are only performed at high temperatures (about 800 ^oC). In addition, incomplete conversion phenomenon of CaO reaction with SO_2 occurs due to pore mouth blockage (gypsum molar volume is very higher than lime, or Z=3). Therefore, lime consumption is high and lime/gypsum mixture cannot be used as a byproduct. On the other hand, Na_2CO_3 can remove SO_2 at low temperatures (about 200 ^oC). Other advantage of Na_2CO_3 FGD system is its lower Z value (Z=1.28), which means high possibility of complete conversion in Na_2CO_3 reaction with SO_2. Consequently, SO_2 removal by Na_2CO_3 can be accomplished in low temperature flue gas ducts and sorbent consumption is low due to complete conversions.

To kinetic studies of non-catalytic gas-solid reactions, several mathematical models such as Modified grain model and RPM have been applied yet. These models can predict alteration of solid structural and specifically partial conversion. Really, industrial sorbents react on the interior areas of pores with a pore size distribution (PSD). Modified grain model simplification assumption is considering of porous solid contains of uniform fine grains which reaction occurs on their surfaces. It was confirmed that RPM accuracy for predicting conversion-time profiles is higher than modified grain model, due to considering of real PSD of the porous sorbent (Bahrami et al. 2015).

As expressed in section 1.2, literature kinetic studies on the reaction of Na_2CO_3 with SO_2 are very scarce. For example, Keener et al. (Keener &Khang 1993) applied sharp interface model for this reaction, while the resulted kinetic parameters seem insecure due to neglecting internal surfaces of sodium carbonate sorbent. On the other hand, Kimura et al. (Kimura &Smith 1987) considered a porous model, while neglecting diffusion resistance between Na_2CO_3 nano-grains is questionable. Ultimately, comprehensive kinetic study of SO_2 reaction with Na_2CO_3 which is not accomplished until now, is highly necessary for determining accurate inherent kinetic parameters. Therefore, the scope of the present work is complete kinetic study of SO_2 reaction with Na_2CO_3 using sophisticated RPM considering concentration dependency and using real PSD of the porous solid. The resulted kinetic parameters are required for design of low temperature FGD reactors.

In this study, to determine the conversion-time profile data of Na_2CO_3 reaction with SO_2, isothermal thermogravimetry was used at predefined concentrations and temperatures. Moreover, precise modelling of Na_2CO_3 reaction with SO_2 is carried out by RPM. To evaluate the PSD, mercury porosimetry and nitrogen adsorption were applied. As well as, the appropriate order of the reaction is estimated. Initial slopes of conversion-time curves at several temperatures are used to determine intrinsic rate constants. The whole conversion-time profiles are employed to estimate the product layer diffusion coefficients. The comparison between measured RPM data and experimental data at various operating conditions displayed good agreement eventually.

2. Materials and Methods

2.1 Raw Materials

To kinetic study of this reaction, pure sodium bicarbonate powder (Chem-Lab) was used as the starting material. 85 mg pellets were constructed in a 10 mm diameter cylindrical mould by 6 bar hydraulic press with 1 mm thickness. The slab pellet was placed in a thermogravimeter and was heated up to temperature range of 100-250 ^oC for 30 minutes. Thus, a porous sodium carbonate pellet ready for reaction with different sulfur dioxide concentrations was prepared by thermal decomposition. The high porosity of the pellet is due to the release of water and carbon dioxide during this calcination step. The gaseous mixture of zero air and SO_2 (99.95 %) was used as a reactant in this study.

2.2 Equipment

A Rheometric Scientific thermogravimeter (TG) was employed in this work that can operate at an isothermal condition with 1^oC deviation. An experimental setup's schematic diagram is provided in Fig. 1. The slab pellets contact better with gaseous stream in TG by placing in a platinum basket. Zero air stream (150 cm^3min^{-1}) was utilized to purge the TG furnace and the sample was heated by a rate of 30 $^oC.min^{-1}$ to attain the reaction temperature. Then, the calcination was carried out in reaction temperature for 30 minutes. As a result, an extremely porous sodium carbonate pellet was provided. Then, in an isothermal step, a mixture of SO_2 and zero air was injected into TG at a pre-

defined concentration. Thus, Na_2CO_3 reacted by SO_2 and TG device measured the weight changes of the pellet at various constant temperatures.

2.3 Sample Characterization

Nitrogen adsorption by Autosorb-1MP from Quantachrome for determination the micro and mesopores of the pellet (by a 55-point test) and mercury porosimetry for evaluation of macropores were utilized to obtain the Na_2CO_3 pellet's whole PSD. Two methods, Horvath-Kawazoe (HK) and Barrett-Joyner-Halenda (BJH), were used for calculating the volume of micropores and mesopores from the nitrogen adsorption test. Furthermore, Washburn equation was used for evaluation of macropores from mercury porosimetry test. Consequently, the whole PSD of the porous Na_2CO_3 pellet in the range of 0.3-1000 nm was obtained which is presented in Fig. 2.

Fig.3 displays the SEM pictures of the raw slab, after calcination at 150 ^oC, after reaction with SO_2 at 150 ^oC (52% conversion), and 225 ^oC (75% conversion). It is obvious from this figure that due to the release of CO_2 and H_2O molecules from the sample, porosity increased after calcination. Then, owing to formation of the product layer around the pores, porosity decreased during the reaction of the pellet with SO_2. In addition, the reduction in the pellet porosity at 225 ^oC is more significant than 150 ^oC, due to the higher reaction rate and higher product layer thickness.

Finally, the XRD pattern of reacted pellet showed both Na_2CO_3 and Na_2SO_4 phases, which emphasized the ability to react and removal of SO_2 by Na_2CO_3.

3. Kinetic Modeling

The most sophisticated RPM model which was originally demonstrated by Bhatia and Perlmutter (Bhatia &Perlmutter 1981) is employed for precise kinetic study by considering different pore diameters and structural alteration (Moshiri et al. 2014, Ramachandran &Doraiswamy 1982). The assumptions of this model are the pseudo-steady state for gas concentration, the irreversible reaction, negligible effect of the bulk flow, the isothermal system and constant size of the pellet (Ale Ebrahim 2010, Bahrami et al. 2014). The dimensionless differential equations for a slab pellet

and an arbitrary concentration dependency are as follows (Bahrami et al. 2014, Bahrami et al. 2016):

$$\frac{\partial}{\partial y}(\delta\frac{\partial a}{\partial y})=\frac{\phi^2 f(a)b\sqrt{1-\psi\ln b}}{1+\frac{\beta Z}{\psi}[\sqrt{1-\psi\ln b}-1]} \quad (2)$$

$$\frac{\partial b}{\partial \theta}=-\frac{f(a)b\sqrt{1-\psi\ln b}}{1+\frac{\beta Z}{\psi}[\sqrt{1-\psi\ln b}-1]} \quad (3)$$

Where, dimensionless gaseous and solid reactants concentration are a and b, the initial Thiele modulus is φ, the main RPM parameter which is the initial pore size distribution's function of the calcined slab is ψ, and the product layer's diffusion resistance is β. The initial and boundary conditions of the above equations are expressed as:

$$\theta=0\rightarrow b=1 \quad (4)$$

$$y=0\rightarrow\frac{\partial a}{\partial y}=0 \quad (5)$$

$$y=1\rightarrow\frac{\partial a}{\partial y}=\frac{Sh}{\delta}(1-a) \quad (6)$$

The local pellet porosity varies by time and described as (Bahrami et al. 2016, Moshiri et al. 2014):

$$\frac{\varepsilon}{\varepsilon_0}=1-\frac{(Z-1)(1-\varepsilon_0)(1-b)}{\varepsilon_0} \quad (7)$$

To relate the dimensionless effective pore diffusion and pellet porosity, following equation is used (Bahrami et al. 2016, Moshiri et al. 2014):

$$\delta=\frac{D_e}{D_{e0}}=(\frac{\varepsilon}{\varepsilon_0})^2=[1-\frac{(Z-1)(1-\varepsilon_0)(1-b)}{\varepsilon_0}]^2 \quad (8)$$

The effective initial pore diffusion (D_{e_0}) is calculated from molecular diffusion determined by the Chapman-Enskog equation (D_{AM}), and Knudsen diffusion equation based on the average pore size (D_{AK}), by the following equations (Bahrami et al. 2016, Liu &Wang 2019):

$$\frac{1}{D_{e_0}} = \frac{1}{\varepsilon_0^2}\left(\frac{1}{D_{AM}} + \frac{1}{D_{AK}}\right) \tag{9}$$

$$D_{AM} = \frac{1.859\times10^{-3}T^{1.5}\sqrt{\frac{1}{M_1}+\frac{1}{M_2}}}{p\sigma_{12}^2\Omega} \tag{10}$$

$$D_{AK} = \frac{2r_{av}}{3}\sqrt{\frac{8R_gT}{\pi M_A}} \tag{11}$$

The main parameters of RPM is computed using the PSD curve by the following equations (Bahrami et al. 2016):

$$V_p = \int_0^\infty v_0(r)dr \tag{12}$$

$$\varepsilon_0 = \frac{V_p}{V_p + \frac{1}{\rho_B}} \tag{13}$$

$$r_{av} = \frac{1}{V_p + \frac{1}{\rho_B}}\int_0^\infty v_0(r)rdr \tag{14}$$

$$S_0 = \frac{2}{V_p + \frac{1}{\rho_B}}\int_0^\infty \frac{v_0(r)}{r}dr \tag{15}$$

$$L_0 = \frac{1}{\pi(V_p + \frac{1}{\rho_B})}\int_0^\infty \frac{v_0(r)}{r^2}dr \tag{16}$$

$$\psi = \frac{4\pi L_0 (1-\varepsilon_0)}{S_0^2} \qquad (17)$$

The resulting structural parameters for the calcinated Na_2CO_3 pellet from $NaHCO_3$ are given in Table 1.

The conversion of slab pellet can be determined as follows (Bahrami et al. 2016, Moshiri et al. 2014):

$$X(\theta) = 1 - \int_0^1 b(y,\theta)dy \qquad (18)$$

In this study, the finite element method is used for solving the coupled nonlinear partial differential equations of RPM.

4. Results and Discussion

4.1 TG and Conversion-Time Results

Typical experimental TG curves of sodium bicarbonate calcination as well as Na_2CO_3 reaction with SO_2 at 150 and 200 ^oC are presented in Figs. 4 and 5. As mentioned pictures show, the first stage were heating of sample pellet under zero air stream to reach the specified reaction temperatures. Through this calcination step, sample weight diminished and porosity of the pellet increased. So a high porous Na_2CO_3 pellet was produced due to release of CO_2 and H_2O which was the reason for about 37% weight loss of initial sample weight. In the next stage, the stream was shifted to a combination of zero air and predefined SO_2 concentration. As a result, the sample weight increased due to the sulfation reaction at isothermal condition of TG. During the reaction, the slope of TG curve decreased gradually because of the product layer's thickness increasing.

4.2 Concentration Dependency Determination

To determine the best reaction's order, several experiments with SO_2 concentrations of 0.13, 0.33, 0.66, and 1.12 vol% were carried out at 150 ^oC. So, the conversion-time data are plotted in Fig. 6. According to this figure, the conversion increased by raising SO_2 mole fraction. As expected, the

pore diffusion and surface reaction controlled the overal rate during the initial stages, while in the next slower stages the reaction rate controlled by product layer diffusion.

Now, the RPM equations were solved by considering $\delta = b = 1$ at zero time to determine the initial conversion-time slopes. Therefore, equation 1 can be simplified to (Bahrami et al. 2016, Moshiri et al. 2014, Rashidi et al. 2013):

$$\frac{\partial}{\partial y}\left(\frac{\partial a}{\partial y}\right) = \phi^2 f\ (a) \qquad (19)$$

The dimensionless gas concentration profile, F(y), inserted in equation 2 and integrated to:

$$b_{\theta \to 0} = 1 - F(y)\theta \qquad (20)$$

As a result, conversion at initial time for a slab pellet by using equation 20 and 18 was obtained as follows:

$$X_{\theta \to 0} = \int_0^1 F(y)\theta dy \qquad (21)$$

The following equation by differentiation of equation 21 at initial time was obtained:

$$\left[\frac{dX}{d\theta}\right]_{\theta \to 0} = \int_0^1 F(y)dy \qquad (22)$$

The dimensionless time was replaced in equation 22 as following (Bahrami et al. 2016, Moshiri et al. 2014, Rashidi et al. 2013):

$$I = \frac{C_{B0}(1-\varepsilon_0)}{S_0 \int_0^1 F(y)dy}\left[\frac{dX}{dt}\right]_{t \to 0} = k_s C_{Ab}^n \qquad (23)$$

In equation 19, $f(a)$ is the power law or fractional concentration dependency. To solve these equations, the numerical analysis with iteration procedure was used. In this study, (I) was plotted versus (C_{Ab}^n) for reaction order between 0.89 and 1.15. The highest regression coefficient was observed in the fractional form. Furthermore, K_{ad} in the denominator was set to get the best results.

$$f(a)=\frac{a}{1+K_{ad}C_{Ab}a} \quad (24)$$

The results are summarized in Table 2. It is clear from this table, that the best regression coefficient is related to fractional concentration dependency. Because of the low SO_2 concentrations $(1>>K_{ad}C_{Ab}\,a)$, the reaction can be assumed first order.

4.3 Rate Constant Estimation

The effect of temperature (in the range of 100-250 °C) on Na_2CO_3 reaction with constant (0.66 vol%) SO_2 concentration is shown in Fig. 7. Conversion improved by elevating temperature owing to increasing the reaction rate. However, conversion decreases above 275 °C owing to the product layer's sintering. The rate constant can be evaluated from the following equation for n=1 (Bahrami et al. 2016):

$$[\frac{dX}{dt}]_{t\to 0}=\frac{k_sS_0C_{Ab}}{C_{B0}(1-\varepsilon_0)}[\frac{\tanh(\frac{L_0}{2}\sqrt{\frac{k_sS_0}{\nu_BD_{e0}}})}{\frac{L_0}{2}\sqrt{\frac{k_sS_0}{\nu_BD_{e0}}}}] \quad (25)$$

The calculated rate constants of Na_2CO_3 reaction with 0.66 vol% SO_2 at different temperatures are reported in Table 3. The frequency factor and activation energy can be evaluated by the Arrhenius plot that is presented in Fig. 8. So, the rate constant was described as follows:

$$k_s=1.8\times10^{-2}\exp(\frac{-22486.04}{RT}) \quad (26)$$

4.4 Product Layer Diffusion Estimation

To obtain the D_p suitable values at various temperatures, the RPM conversion-time curves were plotted by equations 2 and 3 numerically solving and plots was matched with the experimental data. The upward and downward shifts in model conversion-time profiles are gained by higher and lower D_p values, respectively.

Table 4 presents the essential parameters for RPM model at 150 °C. In this table, the low value of Thiele modulus illustrates that the system is not completely controlled by diffusion, and the

accuracy of rate constants is appropriate. Fig. 9 shows a successful comparison between RPM predictions and experimental conversion-time profile at various operating temperatures. As demonstrated in this figure, simulation results predicts experimental data with good agreement.

Table 5 presents the appropriate D_p values. It is obvious that the D_p increases with temperature. The diffusion coefficient's Arrhenius plot is illustrated in Fig. 10. The frequency factor and apparent activation energy were found by regression on this diagram between 100-250 ºC. Thus, the product layer diffusion is described as a function of temperature with the following expression:

$$D_P = 3\times10^{-15}\exp(\frac{-23354.03}{RT}) \qquad (27)$$

5. Conclusion

In this study, the kinetics of sulfur dioxide removal reaction by Na_2CO_3 was comprehensively carried out by RPM. An isothermal TG was employed for experiments between 100-250 ºC and 0.13-1.12 vol% SO_2. The RPM as the most sophisticated mathematical model was applied to generate kinetic parameters of SO_2 reaction by Na_2CO_3. The RPM considers solid reactant PSD, structural changes, solid reactant pore diffusion, and resistance of product layer. Nitrogen adsorption and mercury porosimetry methods were utilized to plot the complete PSD of the sample. The reaction relation with concentration and temperature were investigated by initial slopes procedure. As a result, the first-order concentration relationship can express the kinetics of the reaction with activation energy of 22.5 kJ mol^{-1}. In addition, diffusion coefficients through product layer were specified. RPM predictions follows experimental data with a good agreement. Finally, industrial low temperature FGD plants can be designed by the obtained kinetic parameters.

6. Nomenclature

$a = C_A/C_{Ab}$	Dimensionless gas concentration
$b = C_B/C_{B0}$	Dimensionless solid concentration

C_A	Gaseous reactant concentration in the pellet, kmol m^{-3}
C_{Ab}	Bulk gas concentration, kmol m^{-3}
C_B	Solid reactant concentration, kmol m^{-3}
C_{B0}	Initial solid reactant concentration, kmol m^{-3}
D_{AK}	Knudsen diffusivity, m^2 s^{-1}
D_{AM}	Molecular diffusivity of gas A in the pellet, m^2 s^{-1}
D_e	Effective diffusivity of gas A in the pellet, m^2 s^{-1}
D_{e0}	Initial effective diffusivity of gas A in the pellet, m^2 s^{-1}
D_p	Effective diffusivity of gas A in the product layer, m^2 s^{-1}
k_m	External mass transfer coefficient, m s^{-1}
k_s	Surface rate constant, m s^{-1}
K_{ad}	Adsorption constant, $m^3 kmol^{-1}$
L	Thickness of the pellet, m
L_0	Pore length per unit volume, m^{-2}
M_B	Molecular weight of solid reactant, kg $kmol^{-1}$
M_D	Molecular weight of solid product, kg $kmol^{-1}$
n	Reaction order
r	Pore radius, m
$\bar{r}$	Average pore radius of the pellet, m
R^2	Correlation coefficient
R	Gas constant, J $K^{-1}mol^{-1}$
S_0	Reaction surface area per unit volume, m^{-1}

$Sh = \frac{k_m L}{2D_{AM}}$	Sherwood number for external mass transfer
t	Time, s
$\upsilon_0(r)$	Pore volume distribution function, $m^2\ kg^{-1}$
V_p	Total pore volume, $m^3\ kg^{-1}$
$X\ (\theta)$	Solid conversion at each time
y=2z/L	Dimensionless position in the pellet
z	Distance from the centre of the pellet, m
Z	Ratio of molar volume of solid product to solid reactant
$\beta = 2k_s(1-\varepsilon_0)/(\upsilon_B D_p S_0)$	Product layer resistance
ε	Pellet porosity
ε_0	Initial pellet porosity
$\delta = \frac{D_e}{D_{e0}}$	Variation ratio of the pore diffusion
$\theta = k_s S_0 C_{Ab}^n t\ /[C_{B0}(1-\varepsilon_0] = t\ /\ \tau$	Dimensionless time
ν_B	Stoichiometric coefficient of the solid reactant
ν_D	Stoichiometric coefficient of the solid product
ρ_B	True density of the solid reactant, kg m^{-3}
ρ_D	True density of the solid product, kg m^{-3}
$\phi = (L/2)(k_s S_0 C_{Ab}^{n-1}/\upsilon_B D_{e0})^{1/2}$	Thiele modulus for the pellet
ψ	Main RPM parameter

7. Declarations

Ethics approval and consent to participate: Not applicable

Consent for publication: Not applicable

Availability of data and materials: The datasets used and/or analyzed during the current study are available from the corresponding author on reasonable request.

Competing interests: The authors declare that they have no competing interests.

Funding: No funding was received for conducting this study.

Authors' contributions: Habib Ale Ebrahim is supervisor of this study. Iman Omidi acquired the data. All authors read and approved the final manuscript.

8. References

Ale Ebrahim H (2010): Application of random-pore model to SO2 capture by lime. Industrial & engineering chemistry research 49, 117-122

Bahrami R, Ebrahim HA, Halladj R (2014): Application of random pore model for SO2 removal reaction by CuO. Process Safety and Environmental Protection 92, 938-947

Bahrami R, Ebrahim HA, Halladj R (2015): Comparison of random pore model, modified grain model, and volume reaction model predictions with experimental results of SO2 removal reaction by CuO. Journal of Industrial and Engineering Chemistry 30, 372-378

Bahrami R, Ebrahim HA, Halladj R, Afshar A (2016): A comprehensive kinetic study of the SO2 removal reaction by pure CuO with the random pore model. Progress in Reaction Kinetics and Mechanism 41, 385-397

Bhatia S, Perlmutter D (1981): A random pore model for fluid-solid reactions: II. Diffusion and transport effects. AIChE Journal 27, 247-254

Bland V (1990): Evaluation of dry sodium sorbent utilization in combustion gas SOx/NOx reduction. Electric Power Research Institute

Carson JR (1980): Removal of sulfur dioxide and nitric oxide from a flue gas stream by two sodium alkalis of various sizes.

Charry Prada ID, Rivera-Tinoco R, Bouallou C (2019): Flue gas desulfurization assessment by modeling and experimental work of an optimized fixed-bed NaHCO3 reactor. Industrial & Engineering Chemistry Research 58, 18717-18730

Chen T-M, Wang C-M, Wang I, Tsai T-C (2010): Promoter effect of vanadia on Co/Mo/Al2O3 catalyst for deep hydrodesulfurization via the hydrogenation reaction pathway. Journal of Catalysis 272, 28-36

343 Dal Pozzo A, Moricone R, Tugnoli A, Cozzani V (2019): Experimental investigation of the reactivity of
344 sodium bicarbonate toward hydrogen chloride and sulfur dioxide at low temperatures. Industrial
345 & Engineering Chemistry Research 58, 6316-6324
346 Ebrahimi S, Picioreanu C, Kleerebezem R, Heijnen J, Van Loosdrecht M (2003): Rate-based modelling of
347 SO2 absorption into aqueous NaHCO3/Na2CO3 solutions accompanied by the desorption of CO2.
348 Chemical engineering science 58, 3589-3600
349 Erdos E, Mocek K, Lippert E, Uchytilova V, Neuzil L (1989): Application of the active soda process for
350 removing sulphur dioxide from flue gases. JAPCA 39, 1206-1209
351 ghorbani shahna f, Bahrami A, Rotivand F, Salari S (2017): Evaluation the effects of using surfactants with
352 sodium bicarbonate and limestone for the removal of sulfur dioxide in packed scrubber. Iran
353 Occupational Health Journal 14, 162-151
354 Gray SM, Jarvis JB (2020): Process for removing so2 from flue gases using liquid sorbent injection. Google
355 Patents
356 Han R, Sun F, Gao J, Wei S, Su Y, Qin Y (2017): Trace Na2CO3 Addition to Limestone Inducing High-Capacity
357 SO2 Capture. Environmental science & technology 51, 12692-12698
358 Jia Z, Liu Z, Zhao Y (2007): Kinetics of SO2 removal from flue gas on CuO/Al2O3 sorbent catalyst. Chemical
359 Engineering & Technology: Industrial Chemistry-Plant Equipment-Process Engineering-
360 Biotechnology 30, 1221-1227
361 Keener TC, Khang S-J (1993): Kinetics of the sodium bicarbonate—sulfur dioxide reaction. Chemical
362 Engineering Science 48, 2859-2865
363 Kimura S, Smith J (1987): Kinetics of the sodium carbonate–sulfur dioxide reaction. AIChE journal 33, 1522-
364 1532
365 Kirk RE, Othmer DF, Mann CA (1949): Encyclopedia of Chemical Technology. Vol. II. The Journal of Physical
366 Chemistry 53, 591-591
367 Knight JH (1977): The use of nahcolite for removal of sulfur dioxide and nitrogen oxides from flue gas. The
368 Superior Oil Company
369 Liu C, Wang H (2019): Binary Diffusion Coefficients of Polycyclic Aromatic Hydrocarbons: A Molecular
370 Dynamics Study.
371 Ma W, Haslbeck J (1993): NOXSO SO2/NOx flue gas treatment process Proof-of-Concept test.
372 Environmental progress 12, 163-168
373 Mocek K, Beruto D (1986): On the morphological nature of Na2CO3 produced by thermal decomposition
374 from NaHCO3 and from Na2CO3· 10H2O. Materials chemistry and physics 14, 219-227
375 Mortson M, Telesz RW (2001): Flue gas desulfurization using recycled sodium bicarbonate, The US
376 EPA/DOE/EPRI Combined Power Plant Air Pollutant Control, The Mega Symposium. Citeseer
377 Moshiri H, Nasernejad B, Ebrahim HA, Taheri M (2014): A Comprehensive Kinetic Study of the Reaction of
378 SO2 with CaO by the Random Pore Model. Chemical Engineering & Technology 37, 2037-2046
379 Mousavi SE, Pahlavanzadeh H, Khani M, Ebrahim HA, Mozaffari A (2018): Selective catalytic reduction of
380 SO 2 with methane for recovery of elemental sulfur over nickel-alumina catalysts. Reaction
381 Kinetics, Mechanisms and Catalysis 124, 669-682
382 Petheram L (2002): Acid rain. Capstone
383 Ramachandran P, Doraiswamy L (1982): Modeling of noncatalytic gas-solid reactions. AIChE Journal 28,
384 881-900
385 Rashidi H, Ebrahim HA, Dabir B (2013): Application of random pore model for synthesis gas production by
386 nickel oxide reduction with methane. Energy conversion and management 74, 249-260
387 Sohn HY, Kim B-S (2002): A novel cyclic reaction system involving CaS and CaSO4 for converting sulfur
388 dioxide to elemental sulfur without generating secondary pollutants. 1. Determination of process
389 feasibility. Industrial & engineering chemistry research 41, 3081-3086

Stanislaus A, Marafi A, Rana MS (2010): Recent advances in the science and technology of ultra low sulfur diesel (ULSD) production. Catalysis today 153, 1-68

Tseng H-H, Wey M-Y (2004): Study of SO2 adsorption and thermal regeneration over activated carbon-supported copper oxide catalysts. Carbon 42, 2269-2278

Walawska B, Szymanek A, Pajdak A, Nowak M (2014): Flue gas desulfurization by mechanically and thermally activated sodium bicarbonate. Polish Journal of Chemical Technology 16, 56-62

Wu Y-L, Shih S-M (1993): Intrinsic kinetics of the thermal decomposition of sodium bicarbonate. Thermochimica acta 223, 177-186

Xu G, Luo G, Akamatsu H, Kato K (2000): An adaptive sorbent for the combined desulfurization/denitration process using a powder-particle fluidized bed. Industrial & engineering chemistry research 39, 2190-2198

Yin H, Zhou T, Liu Y, Chai Y, Liu C (2011): NiMo/Al2O3 catalyst containing nano-sized zeolite Y for deep hydrodesulfurization and hydrodenitrogenation of diesel. Journal of natural gas chemistry 20, 441-448

Tables

Table 1- Structural parameters of calcinated Na_2CO_3

Pellet	$\bar{r}\ [cm]$	ε_0	S_0 [1/cm]	L_0 [1/cm^2]	ψ
Calcinated Na_2CO_3	1.92×10^{-5}	0.64	1.27×10^{6}	1.36×10^{12}	3.81

Table 2- Regression coefficients for the concentration dependency

n	0.89	0.9	0.92	0.98	1	1.15	$\frac{C_{Ab}\,a}{1+K_{ad}C_{Ab}\,a}$
R^2	0.9551	0.9510	0.9513	0.9374	0.9326	0.9221	0.97

418

419 **Table 3- Rate constants for SO_2 removal reaction with Na_2CO_3 at various temperatures**

T (°C)	100	125	150	175	200	225	250
k_s (m/s)	8.78×10^{-6}	2.68×10^{-5}	3.48×10^{-5}	5.35×10^{-5}	6.09×10^{-5}	6.65×10^{-5}	9.14×10^{-5}

420

421

422

423

424 **Table 4- RPM parameters for Na_2CO_3+SO_2 reaction at 150 °C**

Parameter	Value
D_{e0} [m^2/s]	2.13×10^{-6}
D_p[m^2/s]	3.40×10^{-18}
ψ	2.12

425

426

427

428 **Table 5- The appropriate D_p values for the reaction of Na_2CO_3 with SO_2 at various temperatures**

T (°C)	D_p [m^2/s]
100	1.25×10^{-18}
125	3×10^{-18}
150	3.4×10^{-18}
175	3.95×10^{-18}
200	6.6×10^{-18}
225	8×10^{-18}
250	1.5×10^{-17}

429

Figures

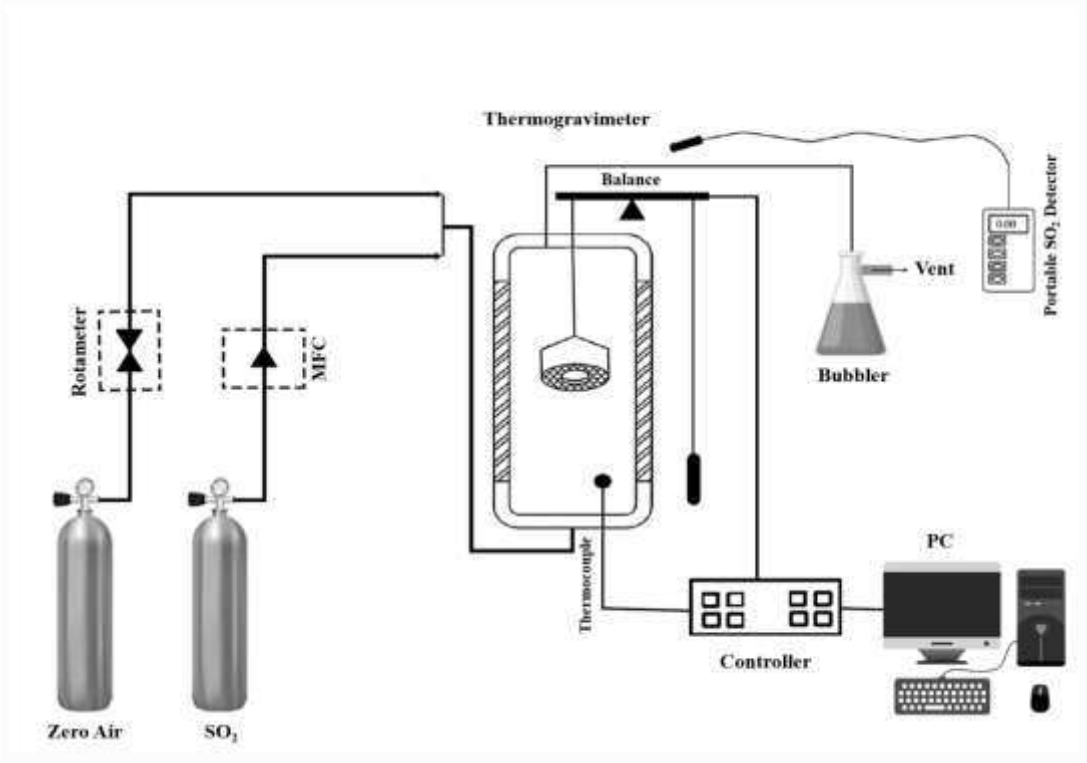

Fig. 1: A schematic diagram of the experimental setup

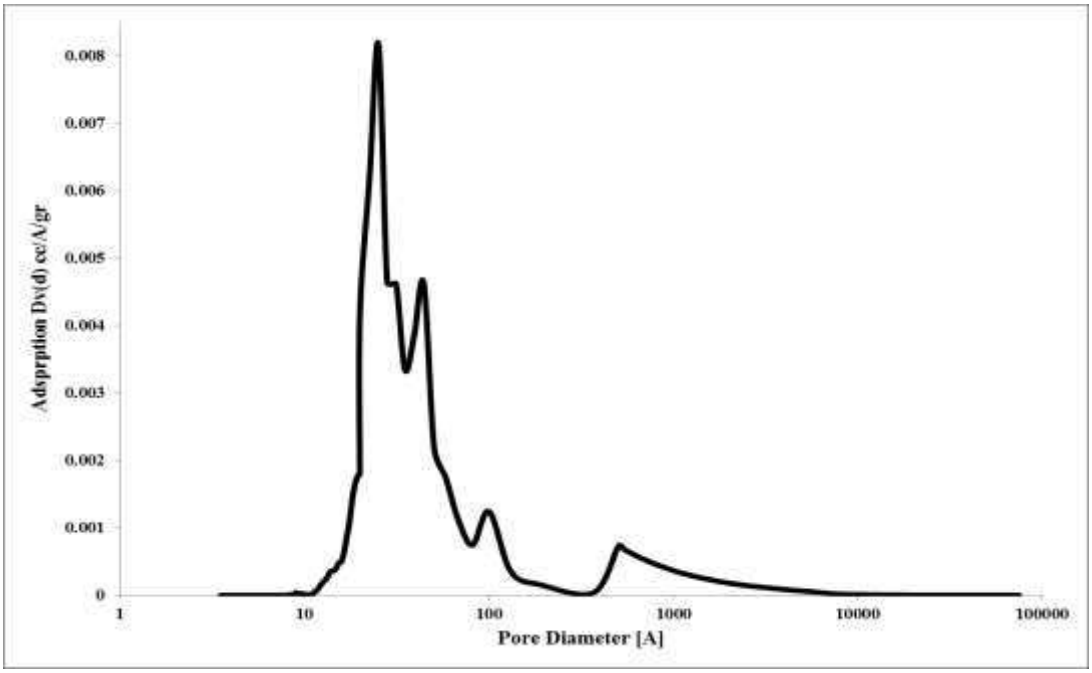

Fig. 2: The whole PSD for Na_2CO_3 pellet

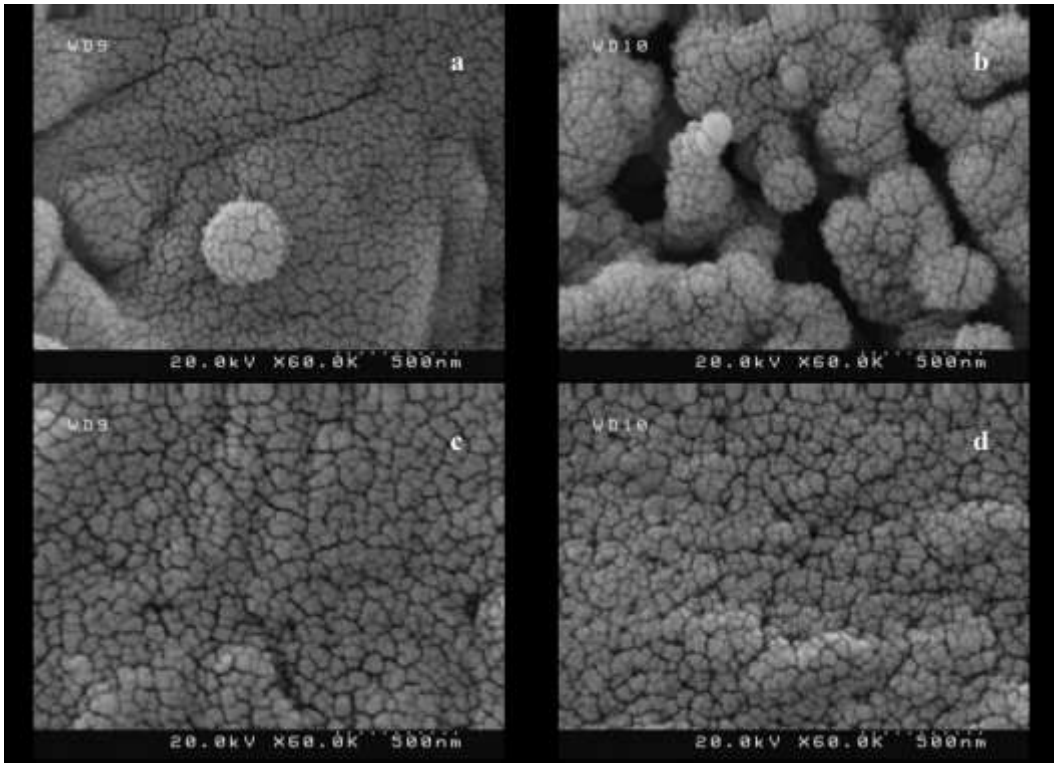

436

437 **Fig. 3: SEM images of the sample (a) before calcination, (b) after calcination at 150 °C, (c) after reaction with SO_2 at 150**
438 **°C, (d) after reaction with SO_2 at 225 °C**

439

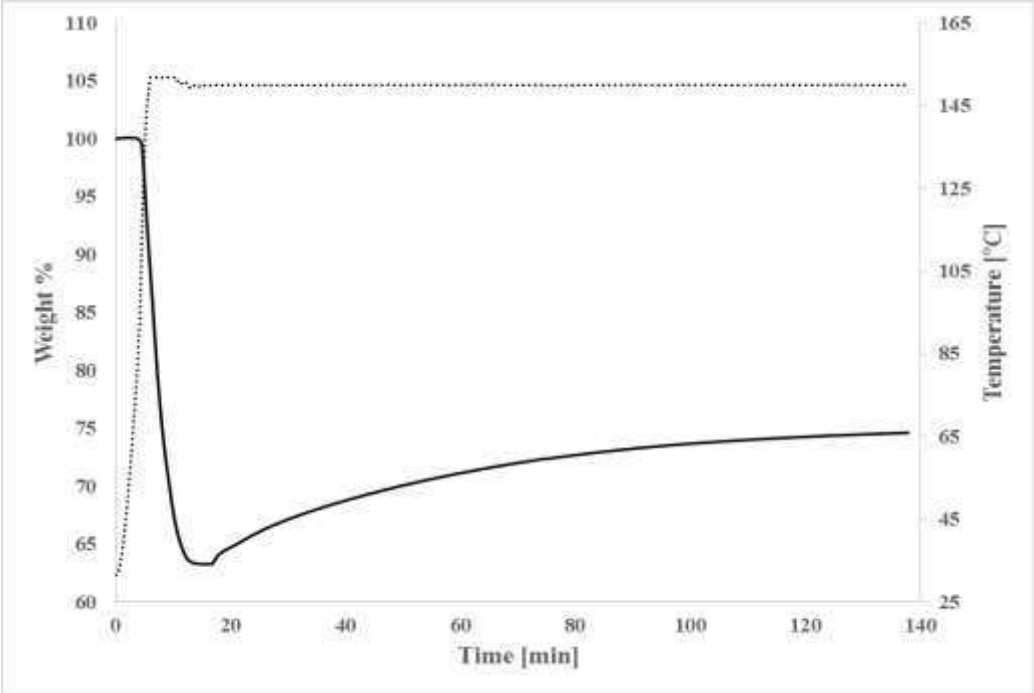

440

441 **Fig. 4: TG curve for sodium bicarbonate calcination and its subsequent reaction at 150 °C and 0.66 vol.% SO_2**

442

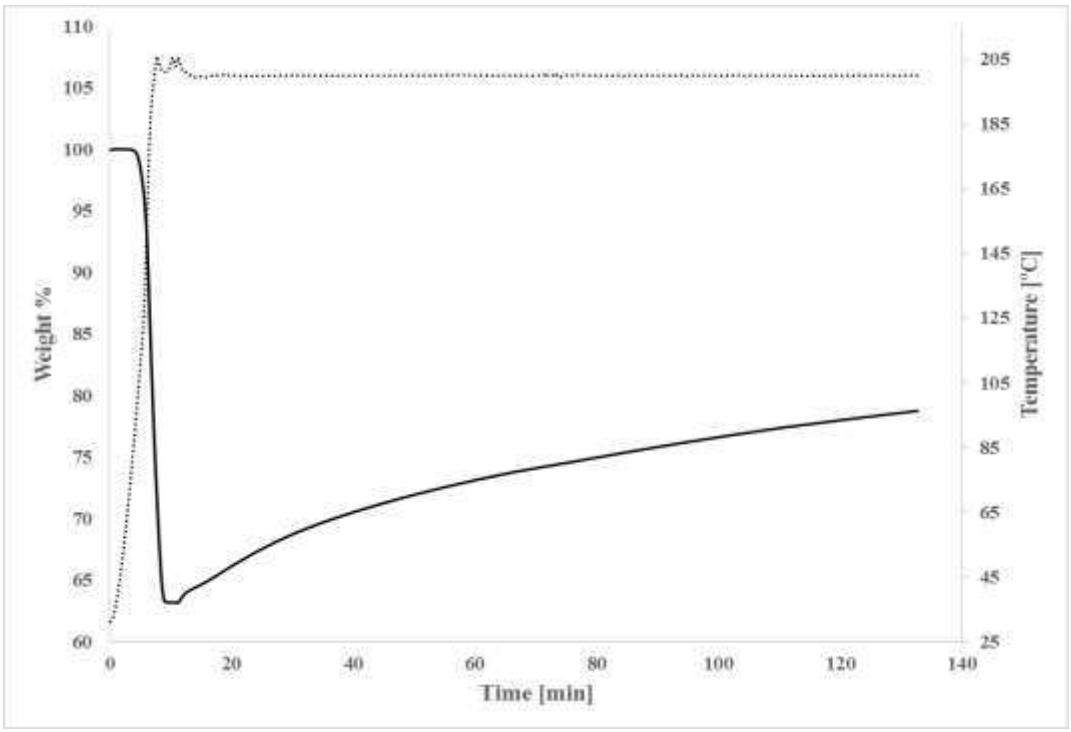

443
444 **Fig. 5: TG curve for sodium bicarbonate calcination and its subsequent reaction at 200 °C and 0.66 vol.% SO_2**
445

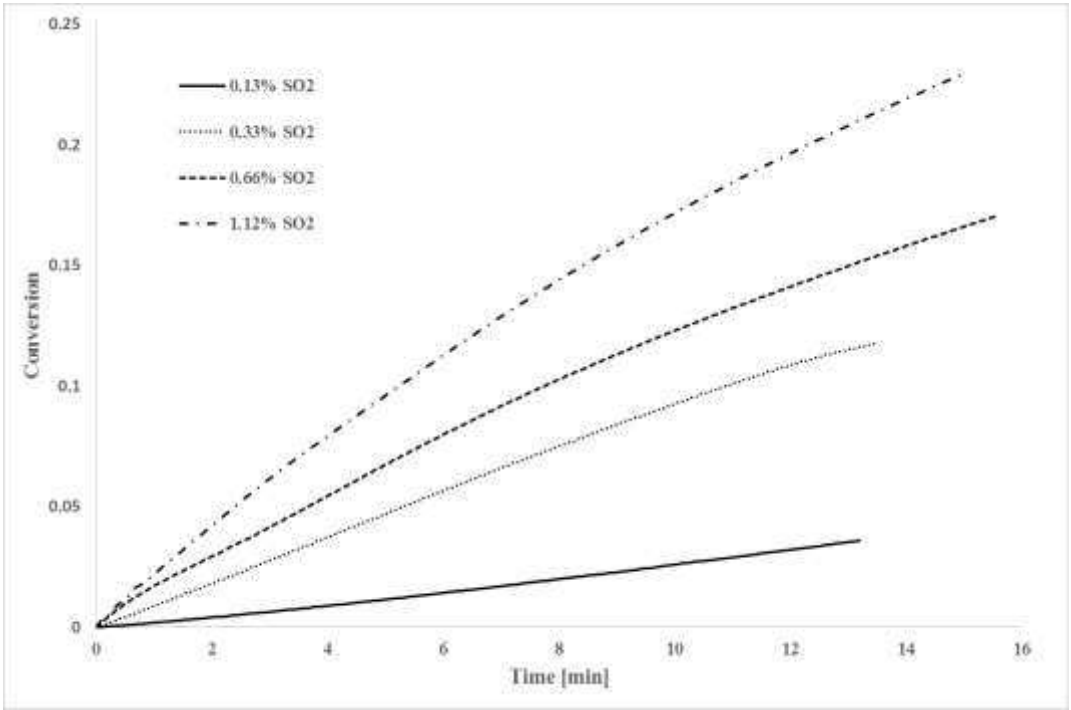

446
447 **Fig. 6: Effect of SO_2 concentration on reaction at 150 °C**

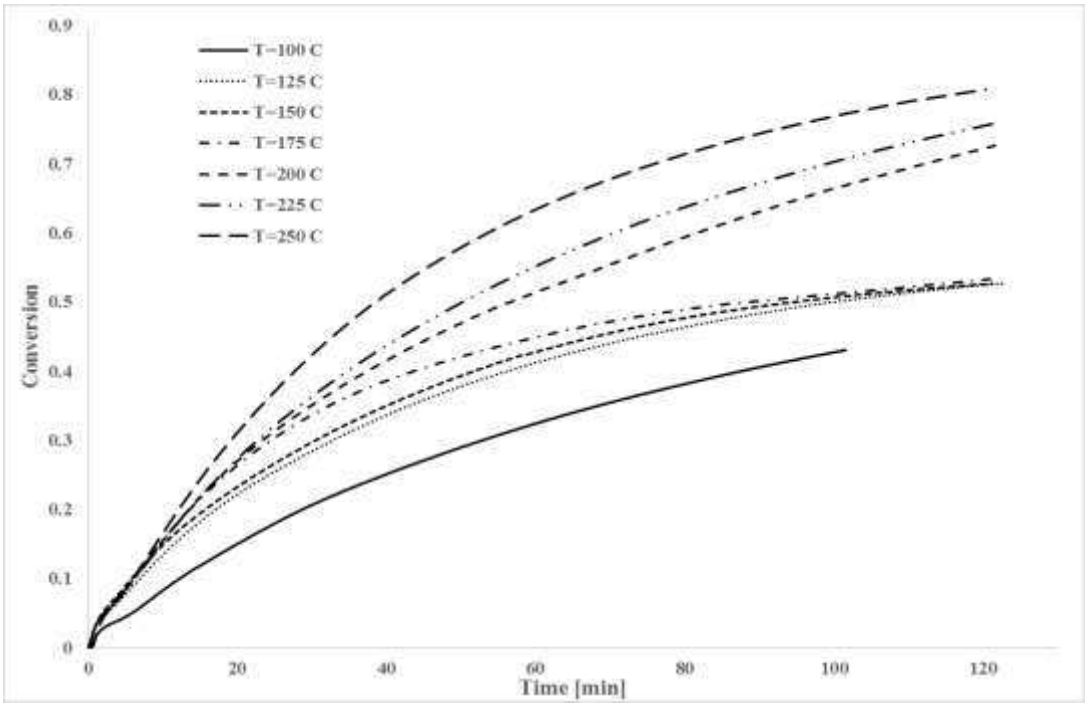

448
449 **Fig. 7: Effect of temperature on reaction at 0.66 vol% SO_2**
450

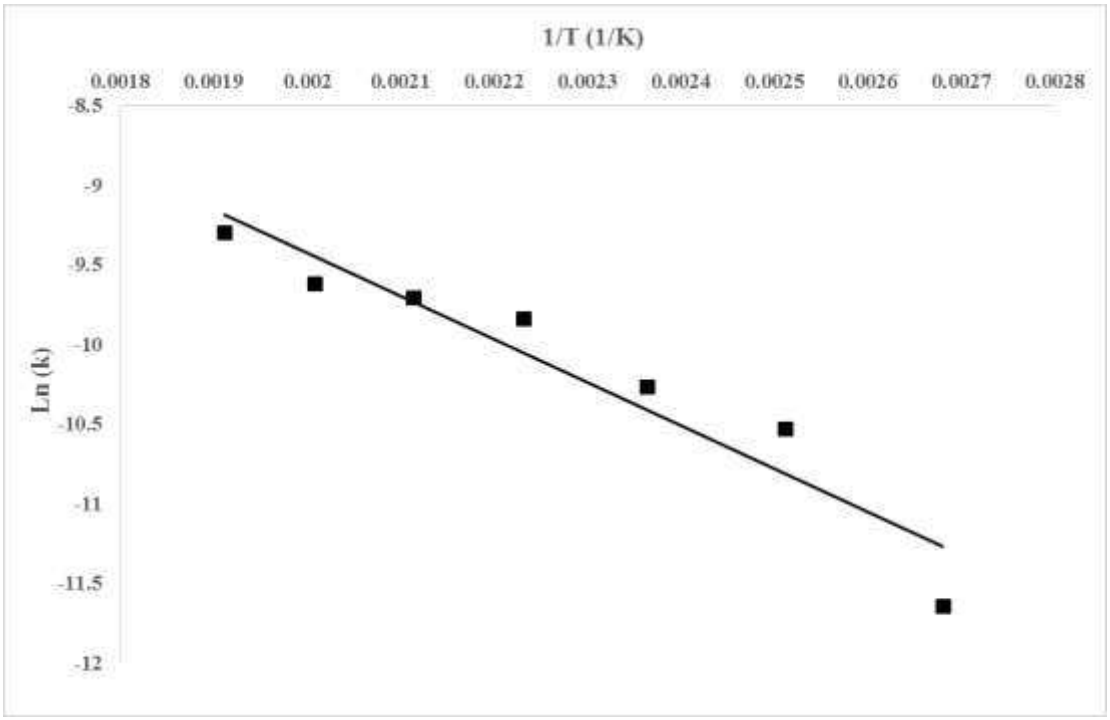

451
452 **Fig. 8: Arrhenius plot on the generated rate constant values**

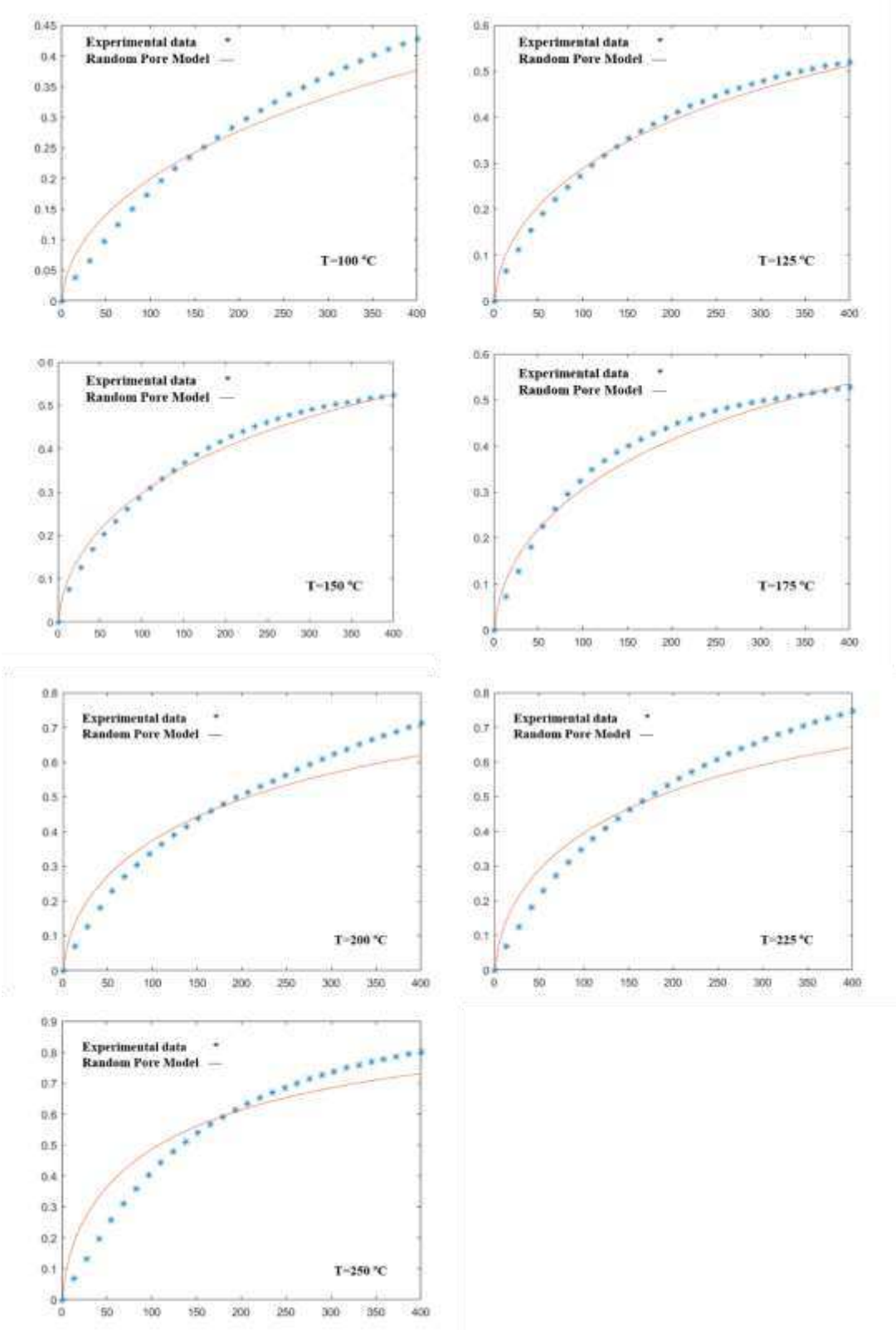

453

454 **Fig. 9: Comparison between predicted data of RPM and experimental data at various temperatures and 0.66 vol% SO_2**

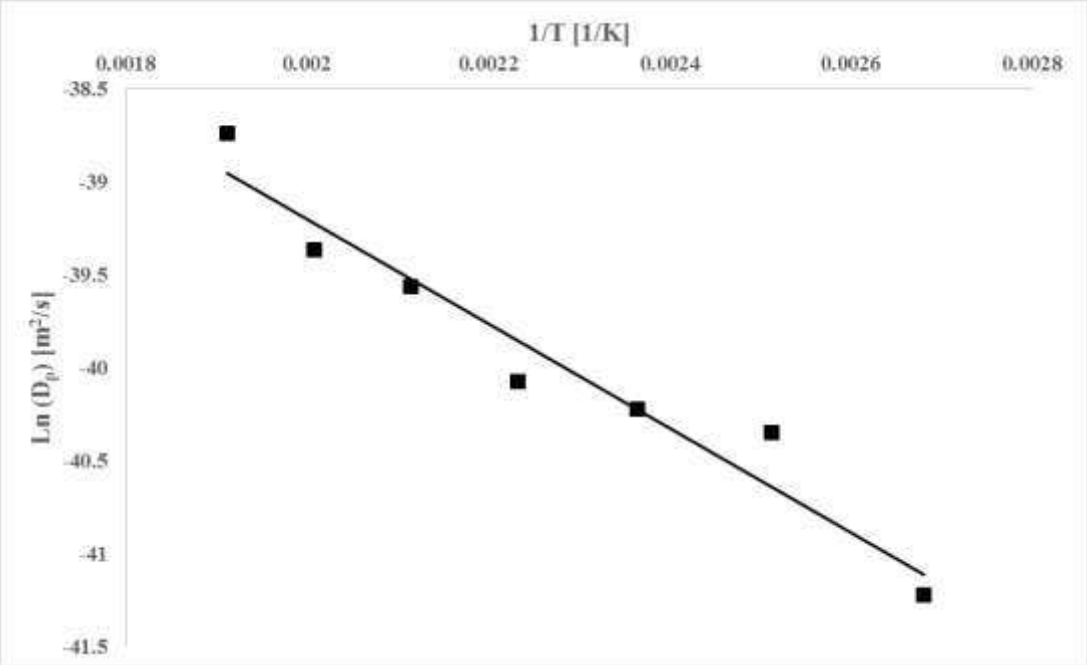

455
456 **Fig. 10: Arrhenius plot on the generated diffusion coefficient values**
457

Figures

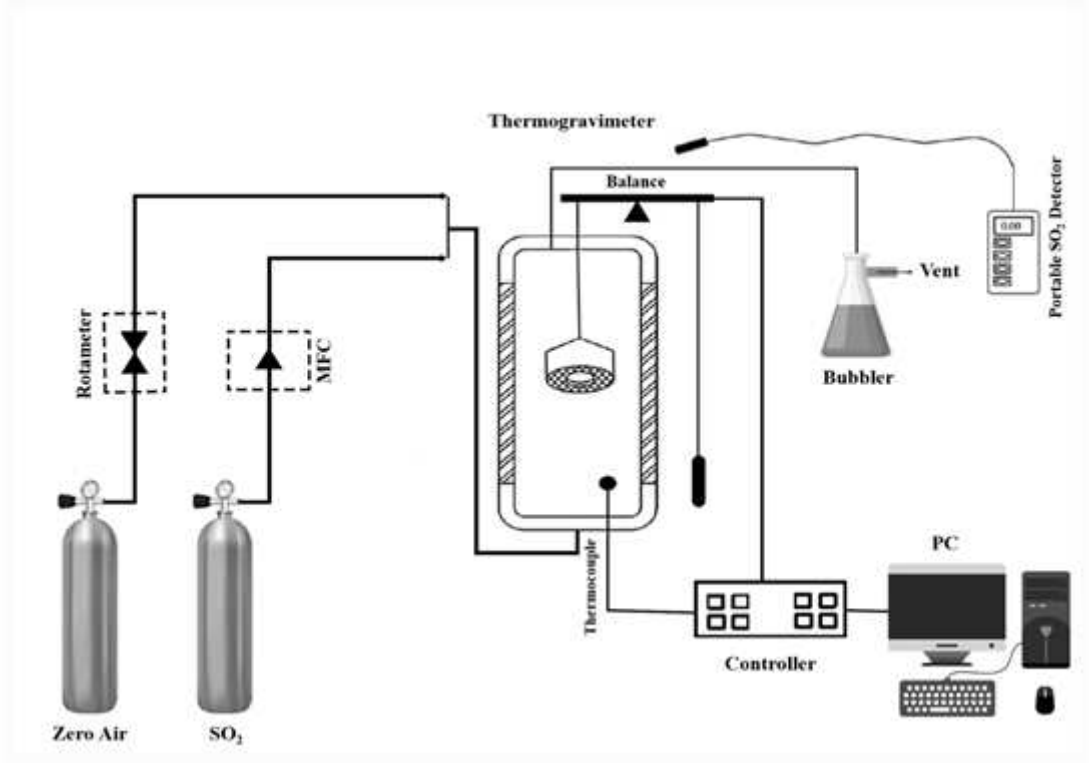

Figure 1

A schematic diagram of the experimental setup

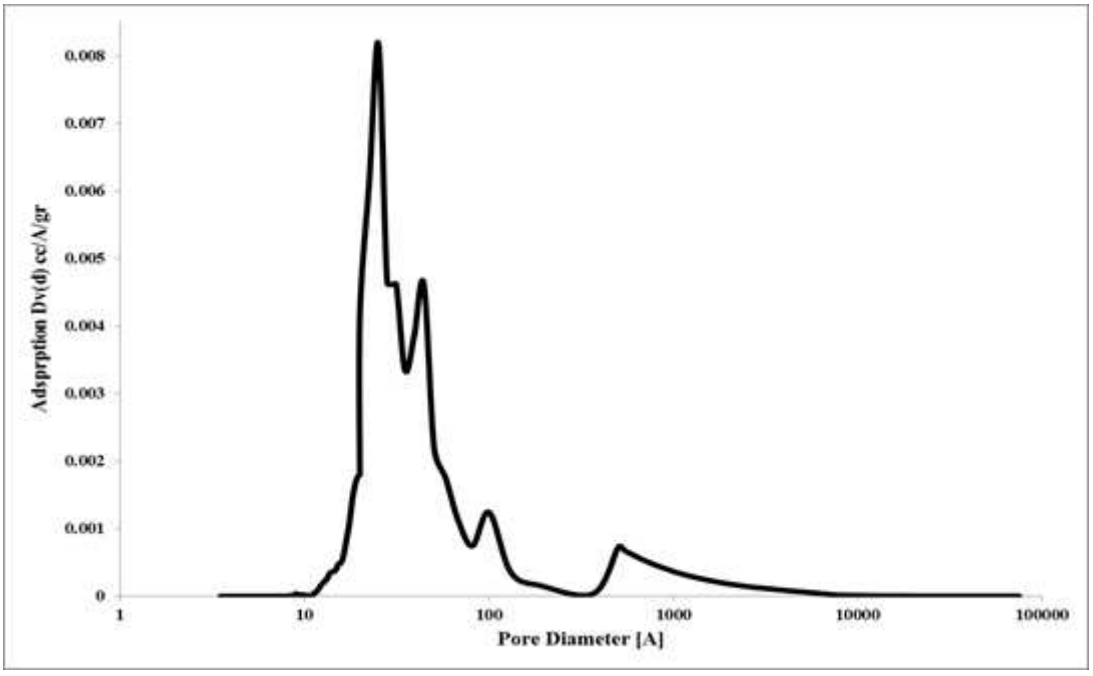

Figure 2

The whole PSD for Na2CO3 pellet

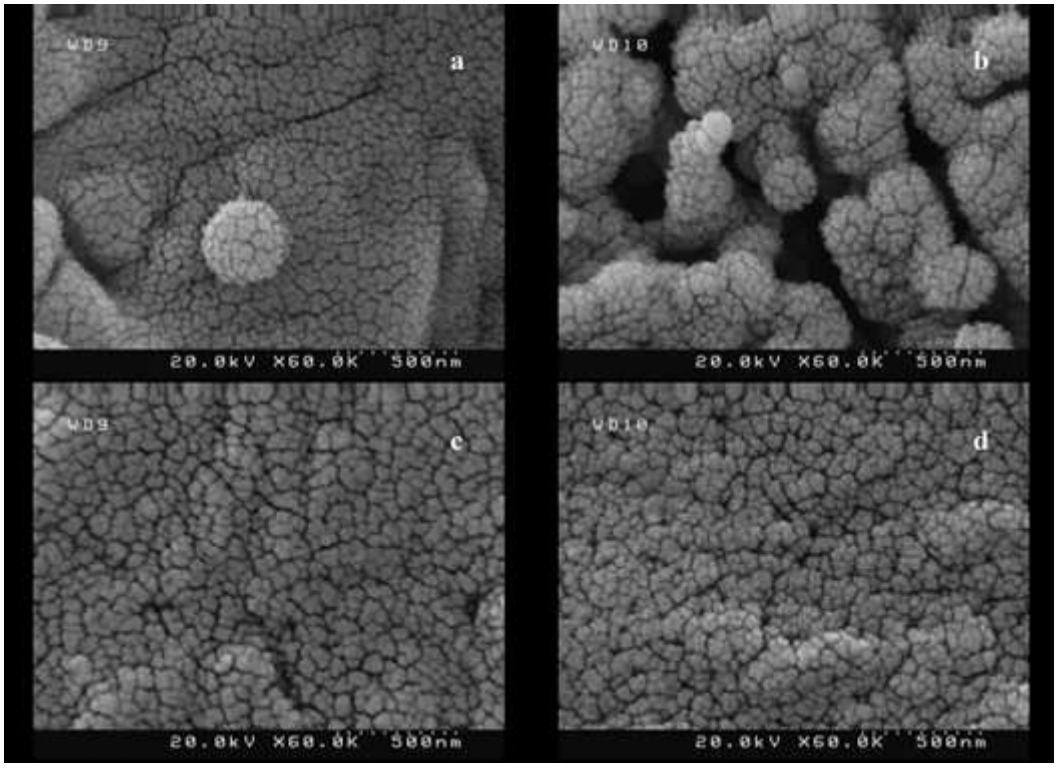

Figure 3

SEM images of the sample (a) before calcination, (b) after calcination at 150 oC, (c) after reaction with SO2 at 150 oC, (d) after reaction with SO2 at 225 oC

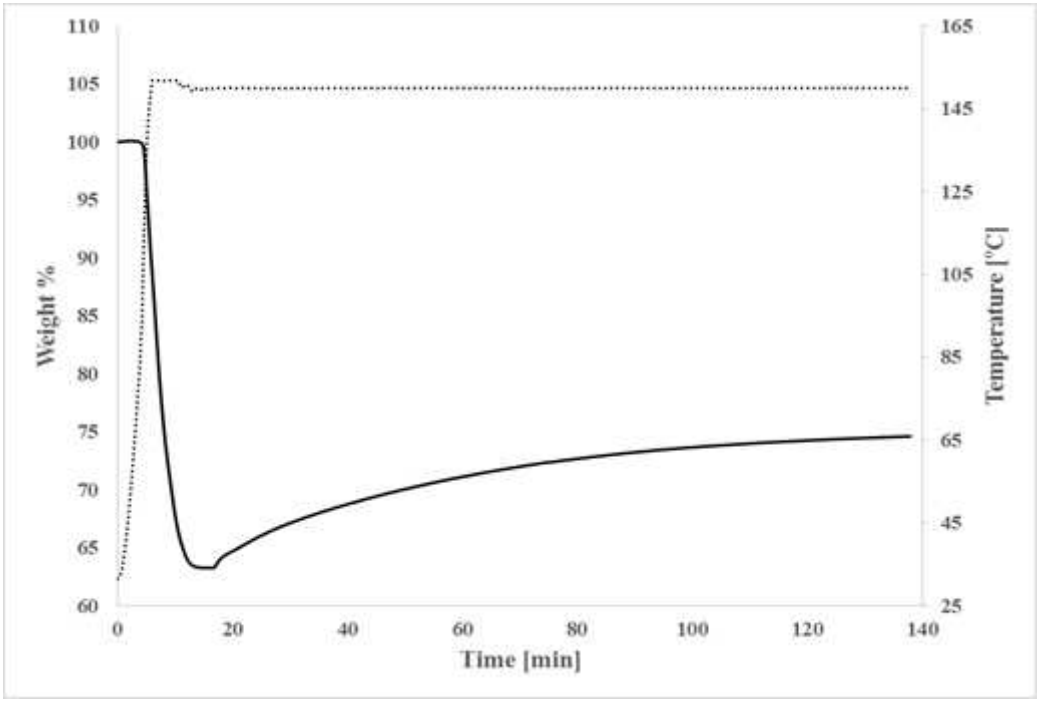

Figure 4

TG curve for sodium bicarbonate calcination and its subsequent reaction at 150 oC and 0.66 vol.% SO2

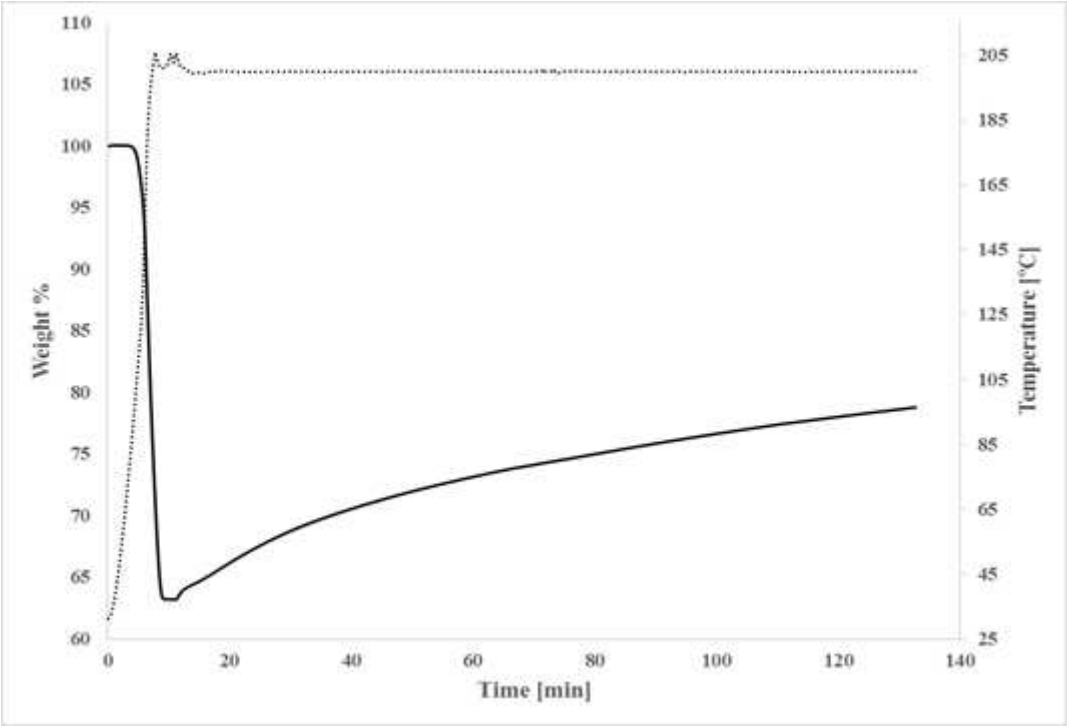

Figure 5

TG curve for sodium bicarbonate calcination and its subsequent reaction at 200 oC and 0.66 vol.% SO2

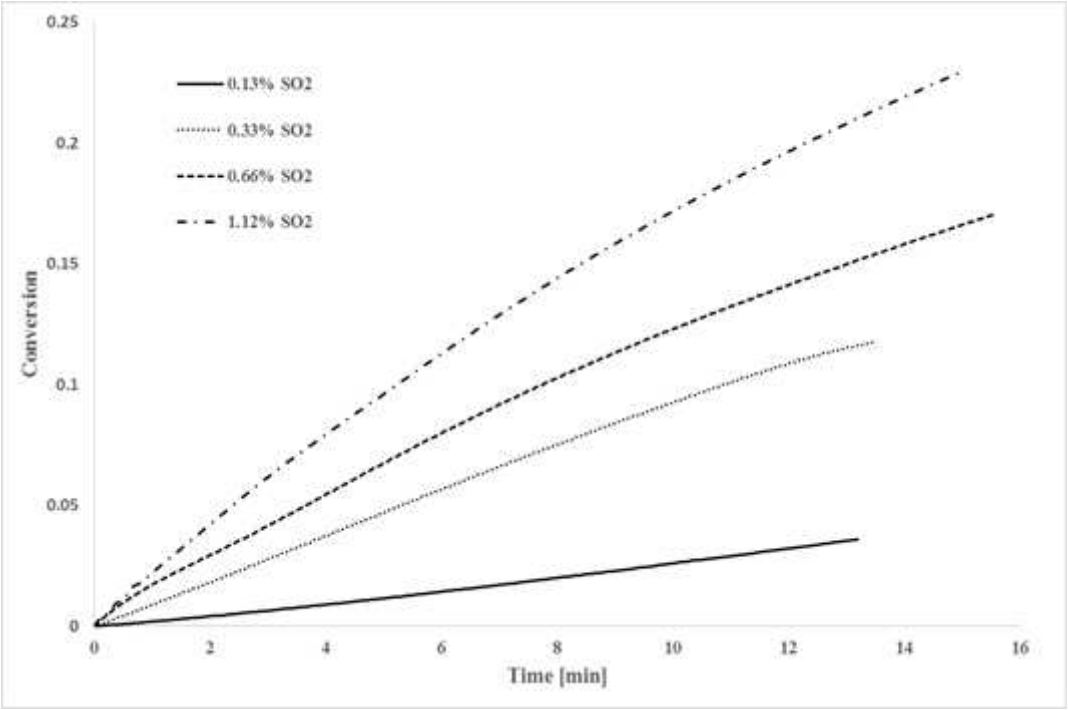

Figure 6

Effect of SO2 concentration on reaction at 150 oC

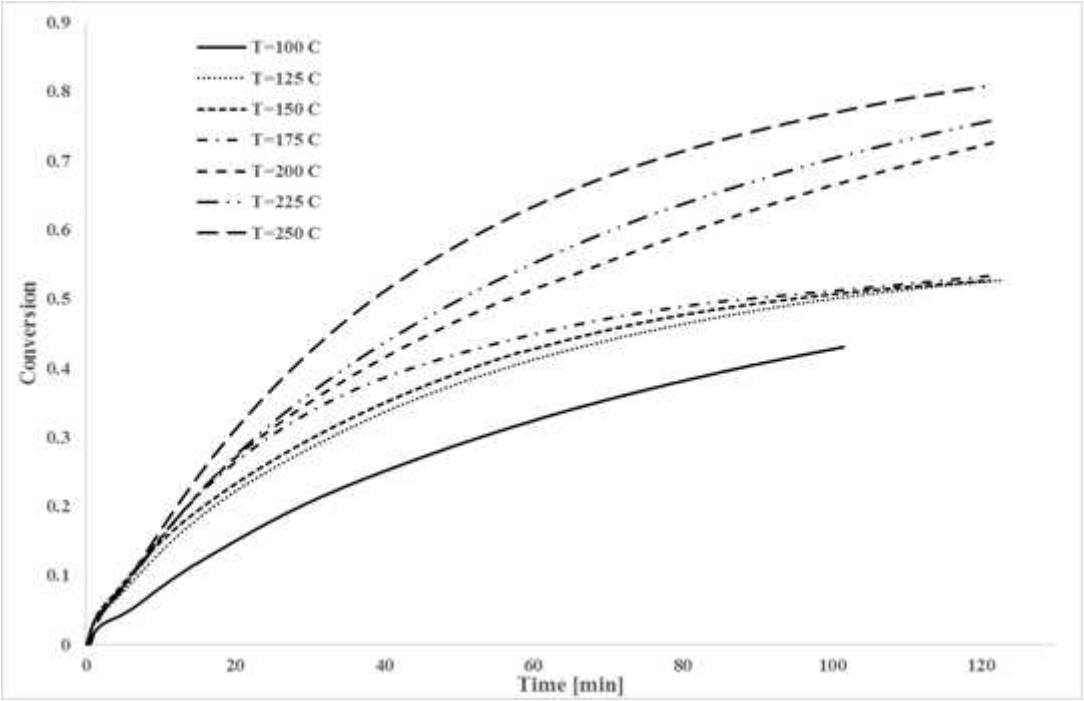

Figure 7

Effect of temperature on reaction at 0.66 vol% SO2

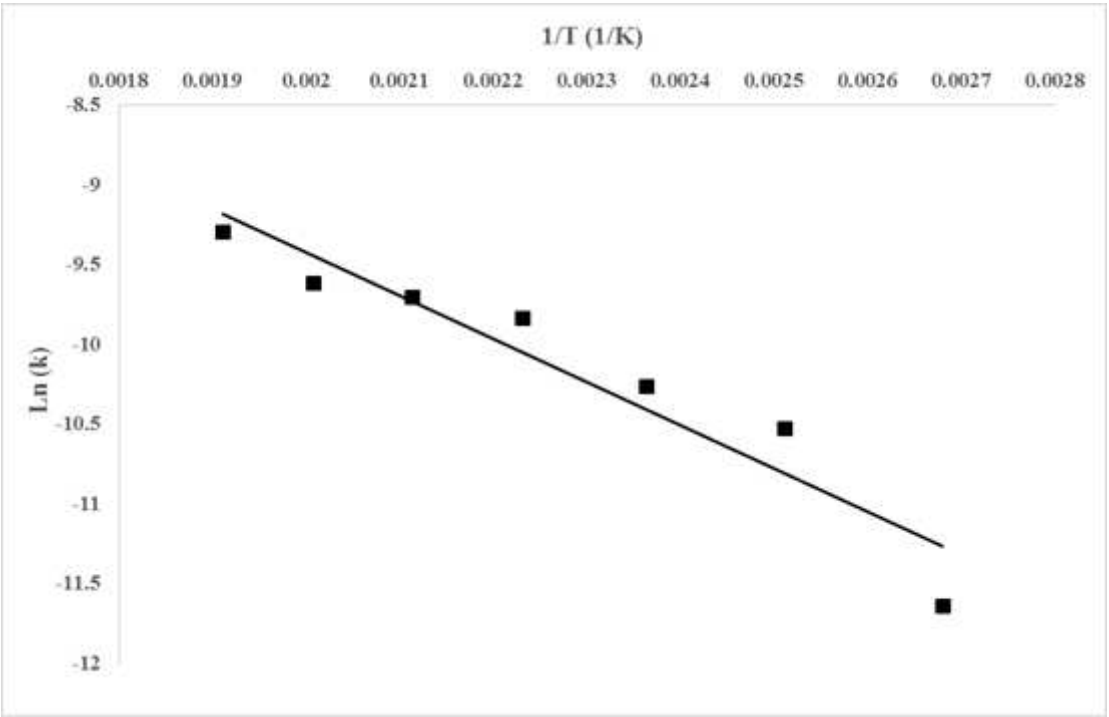

Figure 8

Arrhenius plot on the generated rate constant values

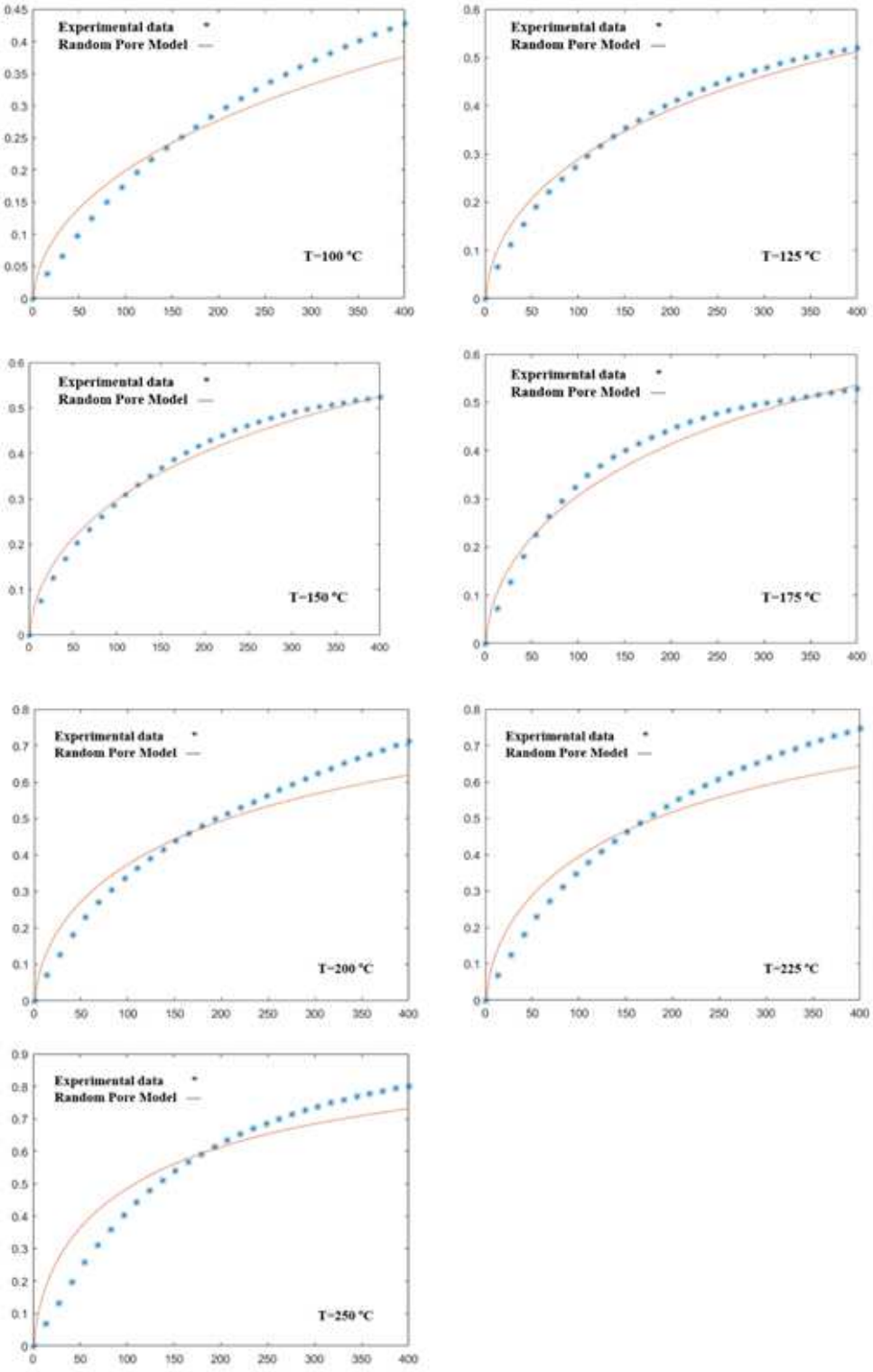

Figure 9

Comparison between predicted data of RPM and experimental data at various temperatures and 0.66 vol% SO2

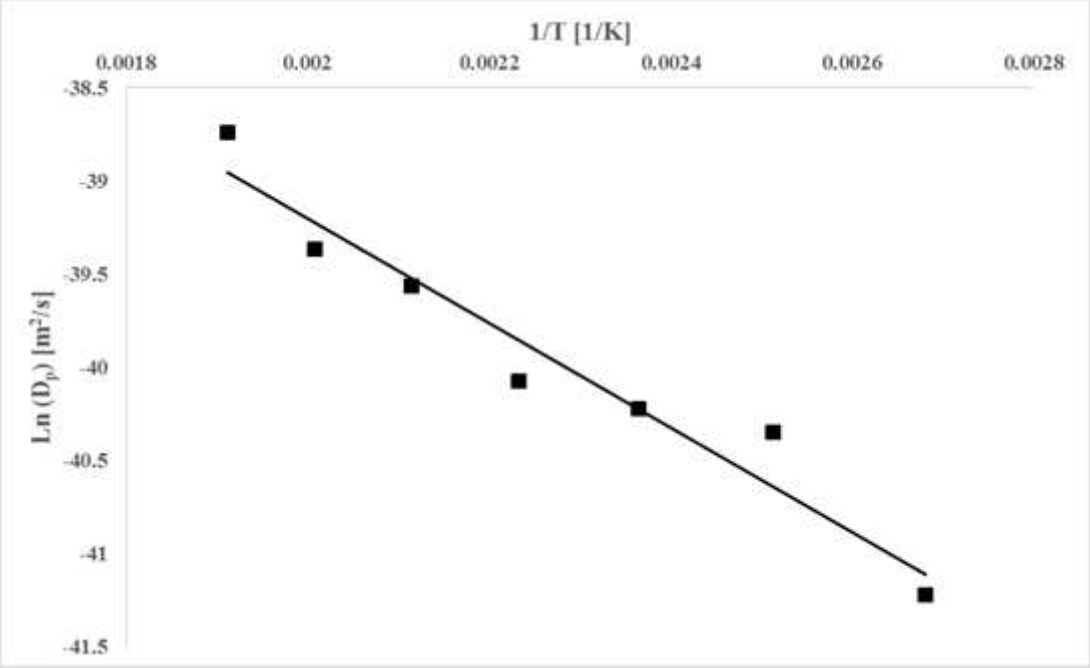

Figure 10

Arrhenius plot on the generated diffusion coefficient values